No detectable precursor in Sentinel-1 backscatter before the 26 August 2026 Langtang Lirung rock–ice avalanche, Nepal

Ajay Kumar Sah

Purbanchal University School of Engineering, Biratnagar, Nepal · ajayshah2005@gmail.com

This is a non-peer-reviewed preprint submitted to EarthArXiv. It has not been submitted to a journal for peer review. Prepared 6 September 2026 · Contains modified Copernicus Sentinel data 2026

Abstract. On 26 August 2026 a rock–ice avalanche on the north face of Langtang Lirung, Nepal, initiated a debris flow and flood that ran roughly 100 km down the Lhende Khola, Bhote Koshi and Trishuli. Several contemporaneous reports asserted that satellite radar had tracked a month of accelerating slope movement before failure; that assertion has not been substantiated in published analysis. Using Copernicus Sentinel-1 IW GRD amplitude on a single relative orbit, this note (i) locates the failure independently and (ii) tests directly for a precursory signal. Co- and cross-polarised change between 16 and 28 August is concentrated on the reported detachment coordinate: within 500 m, 30.0% of VV pixels and 25.4% of VH pixels changed by more than 6 dB, against 0.8% and 0.4% respectively across the remainder of a 308 km^2 scene. Across five pre-event passes from 29 June to 16 August, measured against 80 terrain-matched control patches, VV shows a nominally significant negative trend (−0.20 ± 0.03 dB cycle^{-1} across independent control draws, $p \approx 0.02$) that is produced entirely by the first scene of the series; excluding it, the remaining four dates are flat (+0.01 dB cycle^{-1}, $p = 0.99$). VH shows a monotonic rise (+0.62 ± 0.03 dB cycle^{-1}, $p < 0.01$, robust to exclusion of either endpoint) which is rejected by a same-orbit seasonal baseline: in 2025 the equivalent rise occurred earlier and had completed by late June, whereas in 2026 the face was 3.05 dB below the 2025 plateau at the same date and subsequently rose 2.87 dB. The apparent precursor is the completion of a delayed seasonal transition. No precursory signal is present in the freely available amplitude record at 12-day sampling; the detection limit is approximately 1 dB of progressive change over two months.

Keywords: Sentinel-1, SAR change detection, rock–ice avalanche, precursor detection, Himalaya, Langtang, natural hazards

1. Introduction

The 26 August 2026 failure on Langtang Lirung generated a seismic signal recorded worldwide and initiated a flood that destroyed the Gyirong border crossing and struck settlements along the Trishuli. The event has been described as a rock–ice avalanche rather than a glacial lake outburst, with bedrock failure and the overlying glacier carried with it; the cause remains formally under investigation.

Several early reports stated that satellite radar had detected a month of accelerating movement on the slope before failure. No published analysis supporting that statement could be located.

Because the Copernicus Sentinel-1 archive is open, the claim is directly testable. This note reports that test, together with an independent radar confirmation of the failure location.

2. Data and methods

Sentinel-1 IW GRD products were used as orthorectified gamma-nought (γ^0) in dB, delivered on a fixed WGS 84 grid via Sentinel Hub at approximately 9 m pixel spacing, over a 308 km^2 rectangle (85.446–85.667 E, 28.223–28.351 N) covering the north side of Langtang Lirung and the upper Lhende catchment. All scenes in the primary series are from a single relative orbit acquired at 12:21 UTC, giving identical viewing geometry across dates. Intensities were multilooked with a 5 × 5 boxcar before conversion to dB.

Two series were used. The *event pair* comprises 16 and 28 August 2026, VV and VH. The *pre-event series* comprises six passes at the 12-day repeat: 29 June, 11 and 23 July, 4, 16 and 28 August 2026. A *baseline series* for 2025 (3, 15, 27 June; 9, 21 July; 2, 14, 26 August) and an early-season 2026 series (5, 17, 29 May; 10, 22 June) were acquired from a second relative orbit at 12:22 UTC; these two are mutually same-orbit and are used only in comparison with each other.

2.1 Source polygon and controls

The source polygon was defined exclusively from post-event data as the largest connected cluster of pixels losing more than 6 dB in *both* VV and VH between 16 and 28 August (2,442 pixels, mean elevation 4,898 m, mean slope 39.9°, mean aspect 257°). It therefore carries no information from the pre-event series. Eighty control patches of identical size and shape were drawn at random positions subject to matching within ±6° slope, ±45° aspect, ±2 dB mean pre-event backscatter and ±300 m elevation, all more than 2 km from the source and valid on every date.

Significance is assessed by permutation: the statistic computed for the source is compared against the distribution of the same statistic computed for each control treated in turn as the target. Applying the five-date trend test to control patches yields a false-positive rate of 5.3% against a nominal 5%, indicating the procedure is correctly calibrated. Terrain slope and aspect were derived from SRTM elevation resampled to the radar grid.

2.2 Use of AI-assisted technology

The analysis code used to produce the results and figures reported here, and the initial drafting of this manuscript, were produced with assistance from Claude (Anthropic), a large language model, in an interactive session during September 2026. The model was used to write the processing and statistical code, to generate the figures, and to draft text. All satellite data acquisition and export, the choice of acquisition dates and orbits, and the interpretation of results are the author's. The author has verified the reported values by running the accompanying analysis script, which is archived with the derived data and reproduces every figure quoted in this note from freely available source imagery. The author accepts full responsibility for the content.

3. Independent location of the failure

The largest backscatter change anywhere in the scene coincides with the detachment coordinate reported in early published analysis (28.2853 N, 85.5252 E). Within 500 m of that point, 30.0% of VV pixels and 25.4% of VH pixels changed by more than 6 dB, against 0.7% and 0.4% respectively over the rest of the scene — enrichment factors of 43 and 65. The scene-wide median difference is 0.00 dB, indicating no radiometric offset between acquisitions. A compact zone of backscatter loss (0.25 km^2 confirmed in both polarisations) lies adjacent to a zone of gain (0.05 km^2) to the east-northeast, the expected source-and-deposit configuration.

Because speckle is essentially uncorrelated between polarisations, agreement between VV and VH cannot be produced by noise. Correlation between the VV and VH change fields is 0.80 within 1 km of the site and 0.28 across the remainder of the scene, where speckle dominates. Agreement exceeding 6 dB in both polarisations occurs in 0.065% of pixels away from the site.

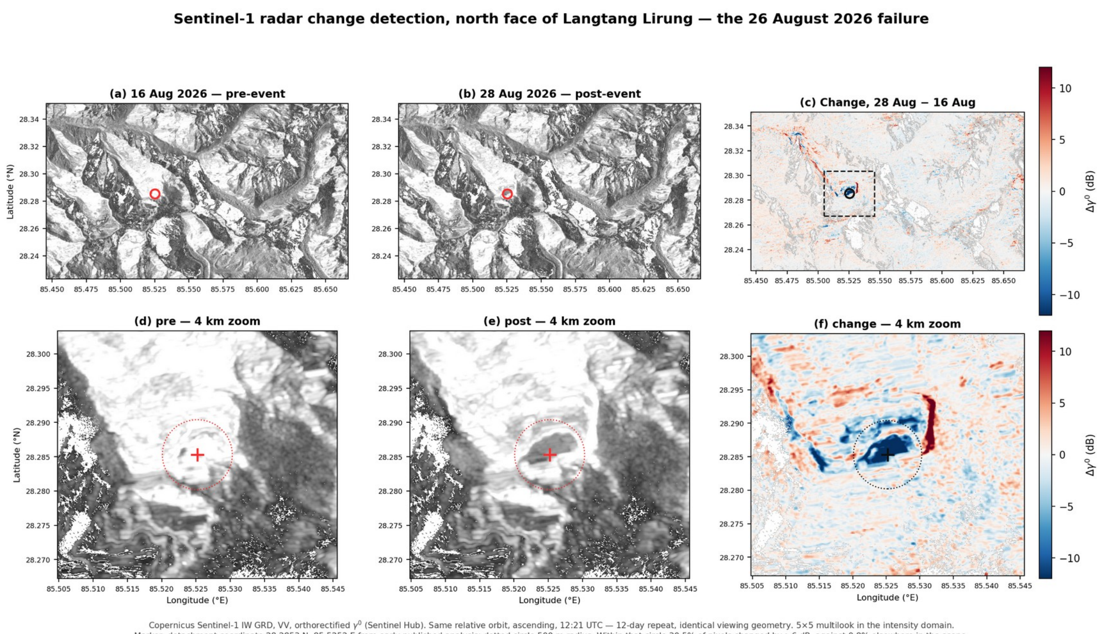

Figure 1. Pre-event, post-event and difference (28 August minus 16 August), VV, with a 4 km zoom. Blue: backscatter loss. Red: gain.

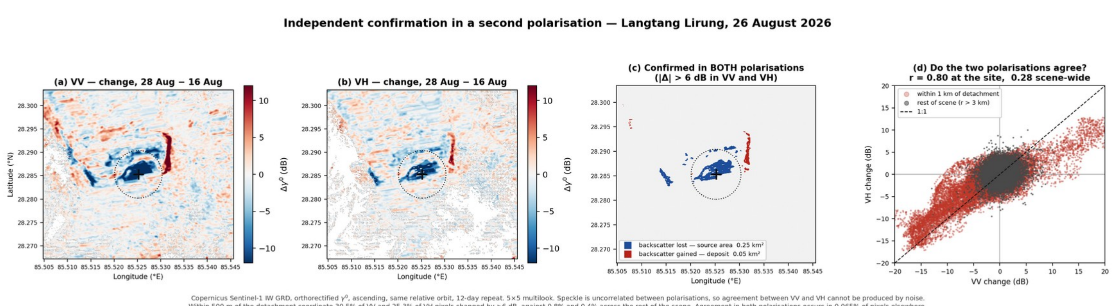

Figure 2. Independent confirmation from the second polarisation, and the correlation structure that distinguishes signal from speckle.

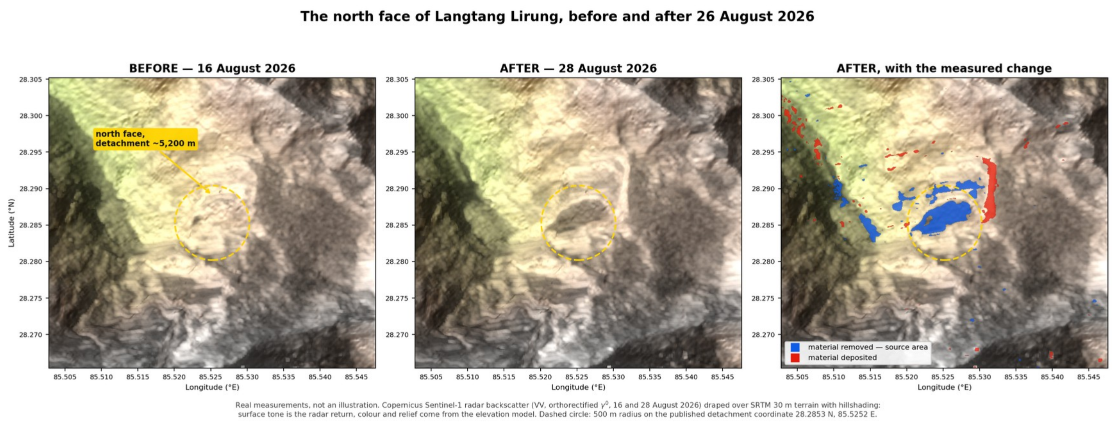

Figure 3. Sentinel-1 VV backscatter draped over SRTM 30 m terrain and hillshaded, before and after, with the detected change overlaid at right. Both layers are measurements.

4. Test for a precursor

4.1 Co-polarised channel

The five pre-event VV anomalies relative to matched controls, expressed as departures from their own mean, are +0.83, −0.22, −0.19, −0.25 and −0.18 dB. A linear fit gives −0.20 ± 0.03 dB cycle^{-1} (mean and standard deviation over five independent control draws), reaching $p < 0.05$ in four of five draws. This is nominally significant but is produced entirely by the first scene: excluding 29 June, the remaining four dates give +0.01 dB cycle^{-1} ($p = 0.99$), that is, flat to within 0.07 dB. The series is not monotonic (Spearman $\rho = -0.30$). The sign is also opposite to that expected of progressive disruption, and there is no acceleration toward failure: the final step, 4 to 16 August, gives $p = 0.31$.

The 29 June scene is the earliest in the series and lies at the end of the seasonal transition discussed in Section 4.2, which is the most plausible explanation for its offset. The event step, 16 to 28 August, is −13.3 dB, 42σ. The test resolves progressive change larger than approximately 0.9 dB over the period; nothing of that magnitude occurred in the co-polarised channel.

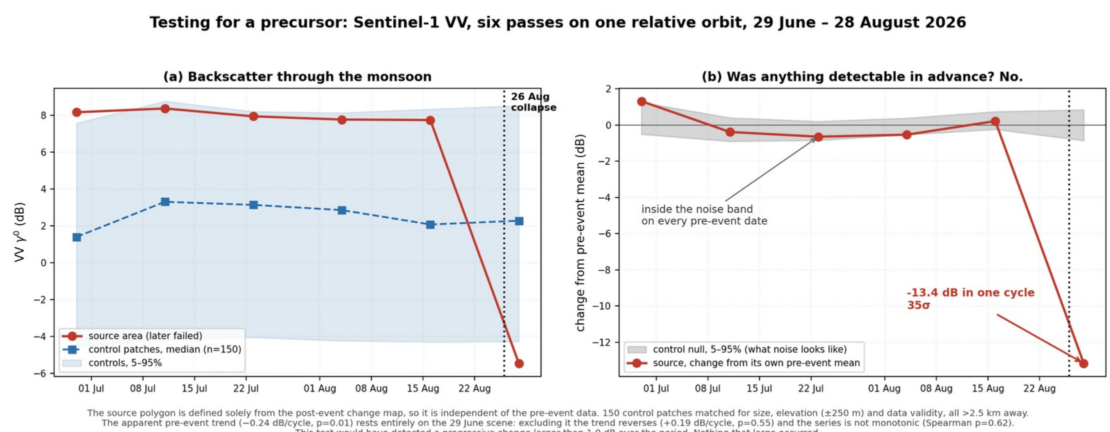

Figure 4. VV time series and anomaly relative to matched controls. The source area remains within the control noise band on every pre-event date.

4.2 Cross-polarised channel and its rejection

VH behaves differently, rising monotonically at +0.62 ± 0.03 dB cycle^{-1} (mean and standard deviation over five independent control draws, $p < 0.01$ in every draw), concentrated on the source polygon (+0.81 dB cycle^{-1}, against +0.07 across the rest of the scene). The trend survives exclusion of the 16 August scene, which is used in defining the polygon and therefore constitutes a potential leakage path (+0.65 dB cycle^{-1}, $p = 0.013$); it is likewise robust to excluding the first scene (+0.55 dB cycle^{-1}, $p < 0.01$). Unlike the co-polarised trend it does not depend on any single date. Since cross-polarised return arises largely from volume scattering, progressive internal fracturing would in principle raise VH while leaving VV unchanged, making this a physically plausible candidate.

A seasonal baseline rejects it. The decisive comparison uses only same-orbit data. Matching by calendar date between 2025, a year with no failure, and the early-season 2026 record:

Quantity	2025	2026
VH anomaly, ~10–15 June	−2.13 dB	−4.14 dB
VH anomaly, ~22–27 June	−0.24 dB	−3.63 dB
Rise over one 12-day June step	+1.89 dB	+0.51 dB
Rise over two cycles to late June	+3.23 dB	+1.34 dB
July–August mean level	−0.58 dB (plateau)	rising, +2.87 dB over the period

Absolute anomaly levels in this table shift by a few tenths of a decibel with the random control draw; the differences between them — the rises and the residual deficit — are stable to within 0.05 dB and carry the argument.

By late June 2025 the seasonal rise had completed and the anomaly plateaued. At the equivalent date in 2026 the face stood 3.05 dB below that plateau and was rising at roughly a quarter of the 2025 rate. Over the subsequent July and August it rose 2.87 dB — approximately the outstanding seasonal deficit. The apparent precursor is therefore the completion of a delayed and slower seasonal transition, most plausibly snowmelt and snowpack metamorphism on the glaciated part of the scene, rather than the onset of a new process. Concentration on the source polygon is expected on the same grounds, since that polygon is glaciated while the control patches are predominantly rock.

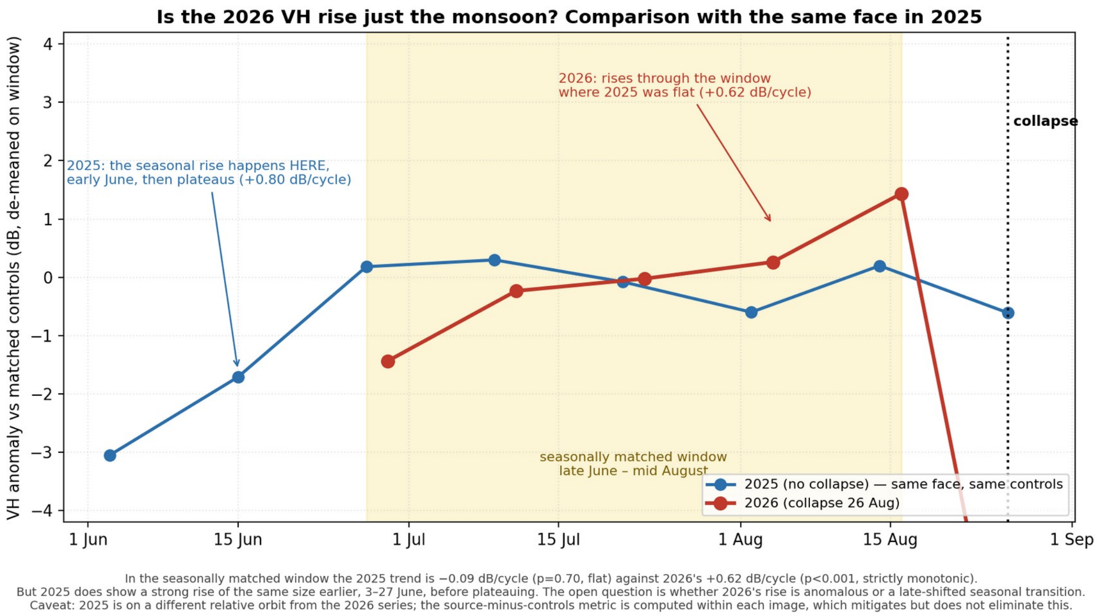

Figure 5. Seasonal baseline comparison. In the matched late-June to mid-August window 2025 is flat and 2026 rises; but 2025's equivalent rise occurred earlier and had completed by late June. The rejection rests on the same-orbit comparison tabulated above; this figure spans two orbits and shows the seasonal shape.

4.3 Sensitivity to the control set

Because control patches are drawn at random subject to matching criteria, results were checked across five independent draws. The VV trend is stable in magnitude (standard deviation 0.03 dB cycle^{-1}) but its p-value straddles the 0.05 threshold between draws, which is why it is reported here with that spread rather than as a single figure. The VH trend is stable in both magnitude (standard deviation 0.03 dB cycle^{-1}) and significance ($p < 0.01$ in every draw). The analysis script accompanying this note reproduces both, and single-draw p-values close to 0.05 should not be read as decisive.

5. Discussion and limitations

Three limitations bound the conclusion. First, radar amplitude responds to surface roughness, geometry and moisture, and is insensitive to slow deformation at the centimetre scale; detecting such motion requires interferometric coherence or phase, which on a snow-covered face at 5,200 m with 12-day repeat would be expected to decorrelate substantially. A negative amplitude result therefore does not demonstrate that no precursory deformation occurred. Second, the 12-day sampling cannot resolve processes shorter than that interval. Third, the reported changed areas are areas of confirmed backscatter change, not mapped failure scars; radar shadow, layover and snow cover bias them, and the 6 dB threshold is arbitrary. A defensible scar outline requires SLC data and coherence analysis.

Within those bounds the result is clear and, because the cross-polarised candidate was found and then rejected, better constrained than a simple null. The specific claim of a month of detectable accelerating movement is not supported by the amplitude record on the correct orbit.

The operational implication is not that higher-performance satellites are required, but that slope-scale ground instrumentation on identified unstable terrain is. The relevant hazard was already documented: Allen et al. (2019) ranked six of the thirty most dangerous glacial lakes on the Tibetan Plateau within Jilong (Gyirong) county, explicitly recognising the transboundary threat to communities downstream in Nepal, and their hazard index includes topographic potential for ice and rock avalanching among its four components, and a supraglacial lake outburst on 8 July 2025 destroyed the Miteri Bridge on the same river. A committee report following that event recommended cross-border early warning, glacial lake monitoring and relocation of high-risk settlements; those recommendations were reported as unimplemented thirteen months later.

6. Data availability

All satellite inputs are freely available from the Copernicus Data Space Ecosystem. Product identifiers for the event pair are `S1D_IW_GRDH_1SDV_20260816T122141` and `S1D_IW_GRDH_1SDV_20260828T122141`. Elevation data are SRTM, obtained as Mapzen / AWS Terrain Tiles. Derived rasters, figures and the analysis code that reproduces every number reported here are archived at Zenodo: Sah, A. K. (2026). Sentinel-1 change detection and precursor test, Langtang Lirung, 26 August 2026: derived data, figures and analysis code (Version 1.0.0) [Dataset]. Zenodo. https://doi.org/10.5281/zenodo.22541072. The Sentinel-1 scenes themselves are not redistributed; the archive README gives the export settings, area of interest and full acquisition list needed to regenerate them from the free Copernicus archive.

Acknowledgements

This work uses modified Copernicus Sentinel data 2026, processed to orthorectified γ^0 by Sentinel Hub. The detachment coordinate used for reference is taken from early published analysis reported in contemporaneous coverage. The author declares no competing interests and received no funding for this work.

Use of AI-assisted technology in preparing this work is disclosed in Section 2.2, in accordance with the ICMJE recommendation that AI use in analysis and figure generation be reported in the methods.

References

1. ICIMOD and Nepal Department of Hydrology and Meteorology — assessments of the 26 August 2026 event, reported August 2026.
2. United States Geological Survey — M 5.2 landslide, 55 km NW of Kodari, Nepal, 26 August 2026, 02:52:10 UTC; and a second landslide event, M 4.2, approximately three hours later. GFZ Helmholtz Centre for Geosciences recorded the main event as Mw 5.7, consistent with a landslide.
3. Nepal Department of Hydrology and Meteorology — preliminary finding of a supraglacial lake outburst in the upper Lhende catchment, 8 July 2025, reported July 2025.

4. Allen, S. K., Zhang, G., Wang, W., Yao, T. and Bolch, T. (2019). Potentially dangerous glacial lakes across the Tibetan Plateau revealed using a large-scale automated assessment approach. *Science Bulletin* 64(7), 435–445. doi:10.1016/j.scib.2019.03.011
5. OnlineKhabar, 1 September 2026 — report on the post-July 2025 committee recommendations and their non-implementation.
6. European Geosciences Union, Hydrological Sciences Division — preliminary volume analysis of the 26 August 2026 event, 28 August 2026.